Enhancing the Accuracy of Jason-3 PWV Products Over Coastal Areas Using the Back Propagation Neural Network

Yangzhao Gong and Zhizhao Liu, *Member, IEEE*

***Abstract*—The performance of microwave radiometers aboard altimetric satellites in measuring water vapor degrades significantly over coastal areas due to the mixing of land within its footprint. In this study, we propose using the back propagation neural network (BPNN) models to enhance the accuracy of Jason-3 precipitable water vapor (PWV) over coastal areas. PWV data from 2076 globally distributed coastal and island Global Navigation Satellite System (GNSS) stations and 237 radiosonde stations are used as the reference. Specifically, the GNSS PWV data in 2016 and 2017 are used to train the BPNN models, while the GNSS and radiosonde PWV observations from January 2018 to June 2023 are used to test the performances of the BPNN models proposed. Our results show that the proposed BPNN PWV models can considerably enhance the accuracy of Jason-3 PWV recorded in the coastal areas (within 25 km of land). Evaluated by the GNSS PWV, BPNN models can reduce the root mean square error (RMSE) of Jason-3 PWV in the coastal areas from 4.2 to 2.7 kg/m^2 (35.7% of RMSE reduction). Assessed by the radiosonde PWV, the results indicate that the RMSE of Jason-3 PWV in the coastal areas is decreased from 5.0 to 3.6 kg/m^2 (28.0% of RMSE reduction) after using the proposed BPNN models.**

***Index Terms*—Back propagation neural network (BPNN), coastal areas, Jason-3, precipitable water vapor (PWV).**

I. Introduction

PRECIPITABLE water vapor (PWV) in the atmosphere causes considerable signal transmission delays for altimetric satellites [1], [2], [3], [4]. Normally, 1 kg/m^2 of PWV will lead to 6 to 7 mm of altimetry signal wet delay [5]. The altimetric satellite signal wet delay typically varies between 0 and 50 cm in the zenith direction [6], which largely limits the performance of altimetric satellites in monitoring the sea level anomaly. To mitigate the impact of water vapor and further obtain more accurate sea level height observations, altimetric satellites, such as Jason satellite series, Sentinel-3A and 3B satellites, and Haiyang (HY)-2B satellite, normally carry a microwave radiometer that can measure the amount of water vapor between the satellite and sea level. The altimetry-based microwave radiometer can measure PWV with high accuracy in open sea areas, e.g., no more than 1.9 kg/m^2 of root mean square error (RMSE) between Jason-3 PWV and shipborne Global Navigation Satellite System (GNSS) PWV [7]. However, due to the large difference in emissivity between land and water, the performance of a microwave radiometer degrades significantly when the altimetric satellite approaches land areas and its footprint covers both land and ocean areas [3], [8], [9]. For example, when the distance of the Jason-2 satellite to land is less than 25 km, the Jason-2 observations with significant land contamination will be flagged as invalid data [8].

In the altimetry community, most of the previous studies focused on enhancing the accuracy of wet delay corrections rather than PWV observations in coastal areas. Brown [8] proposed a wet delay retrieval algorithm for the advanced microwave radiometer (AMR) on Jason-2 altimetric satellite. This algorithm was estimated to be able to achieve a wet delay retrieval accuracy better than 1.5 cm in the coastline. Recently, Aguiar et al. [10] developed a neural network algorithm for Sentinel-3A satellite wet delay retrieval over coastal areas. Their results showed that, when the distance of Sentinel-3A is less than 5 km from the coast, the algorithm proposed can estimate wet delay with an accuracy of 3.3 cm, while the wet delay retrieval accuracy of Sentinel-3A operational algorithms is 16.2 cm. In addition, a couple of previous studies have adopted the neural network algorithms for altimetry wet delay correction retrieval in open areas [11], [12], [13], [14]. These studies all showed the effectiveness of neural network algorithms in retrieving wet delay corrections. However, there were few studies working on enhancing the quality of altimetric satellite PWV data in coastal areas.

In this study, we focus on improving the accuracy of PWV observations from Jason-3 altimetric satellite in coastal areas as PWV is an important atmospheric parameter for not only ocean altimetry but also for atmospheric science [15] and many other fields. In recent years, using ground-based GNSS PWV to enhance satellite-based PWV accuracy has attracted increasing attention [16], [17], [18], [19], [20], [21], [22]. On the one hand, several studies utilized GNSS PWV data as reference observations to develop accurate satellite PWV retrieval algorithms by establishing the relationship between GNSS PWV and the parameters employed in satellite PWV retrieval [16], [17]. For

Received 15 November 2024; revised 3 February 2025; accepted 4 April 2025. Date of publication 16 April 2025; date of current version 29 April 2025. This work was supported by the Hong Kong Research Grants Council (RGC) under Grant PolyU 15221620/B-Q80Q, Grant PolyU 15205821/B-Q84W, and Grant PolyU 15212622/B-Q94L, in part by the Otto Poon Research Institute for Climate-Resilient Infrastructure, and in part by The Hong Kong Polytechnic University (PolyU) RICRI, project code ZH8Y. *(Corresponding author: Zhizhao Liu.)*

The authors are with the Department of Land Surveying and Geo-Informatics, The Hong Kong Polytechnic University,, Hong Kong (e-mail: 18105647r@connect.polyu.hk; lszzliu@polyu.edu.hk).

Digital Object Identifier 10.1109/JSTARS.2025.3559732

example, He and Liu [17] proposed a novel PWV retrieval algorithm for the Moderate Resolution Imaging Spectroradiometer (MODIS) instrument by modeling the relationship between GNSS PWV and the transmittances at MODIS near-infrared absorption bands. Their results indicated that the proposed retrieval algorithm improved the MODIS PWV accuracy by 45.34% to 53.06% compared with the MODIS official PWV products. On the other hand, some studies used GNSS PWV as reference data to calibrate satellite-based PWV data in official products [18], [19], [20], [21]. Xiong et al. [18] adopted three machine learning methods, i.e., random forest, generalized regression neural network, and back propagation neural network (BPNN), to calibrate MODIS PWV in China for the year 2019. GNSS PWV was used as the reference to train their PWV calibration models. They reported that calibrated by GNSS PWV, the RMSE of MODIS PWV was reduced from 5.8 to 3.3 kg/m^2. Xu and Liu [20] applied six different machine-learning methods including the BPNN model to improve the accuracy of MODIS PWV products in Australia. Their results indicated that the MODIS PWV accuracy was improved by 37.81% to 55.25%. The results from the previous studies encourage us to utilize accurate coastal/island GNSS PWV to enhance the accuracy of water vapor observations for altimetric satellites over coastal areas.

So far very few studies have been reported to apply GNSS PWV in collaboration with neural network models to enhance the altimetric satellites' PWV observations in coastal areas. In this study, two BPNN PWV models are proposed to enhance the accuracy of Jason-3 PWV products over coastal areas. The BPNN algorithm is selected as previous studies have demonstrated the effectiveness of the BPNN algorithm in PWV retrieval [23], [24]. PWV data collected from 2076 coastal GNSS stations worldwide in 2016 and 2017 are used to train the BPNN models, while GNSS and radiosonde PWV from January 2018 to June 2023 are utilized to assess the performances of the BPNN PWV models.

The remaining part of this study is organized as follows. First, the Jason-3 data, GNSS PWV, and radiosonde data are introduced in Section II. Then, the description of the BPNN PWV models is given in Section III. The results and related analyses are shown in Section IV. Finally, Section V concludes the article.

II. Jason-3, GNSS, and Radiosonde Data

A. Jason-3 Data

Jason-3 altimetric satellite, launched on 17 January 2016, is the successor to TOPEX/Poseidon, Jason-1, and Ocean Surface Topography Mission/Jason-2. It is designed to measure the height of sea surface via a radar altimeter [4], [25]. To provide accurate wet delay corrections for the altimeter signals, Jason-3 is equipped with an AMR-2 that can measure the water vapor information along its trajectory [26]. Jason-3 AMR-2 operates at three different channels, i.e., 18.7, 23.8, and 34 GHz. The 23.8 GHz channel is the primary water vapor sensing channel, while the other two channels are applied to remove the impacts of cloud liquid water and sea surface roughness.

In this study, Jason-3 final geophysical data records (GDR-F version) level-2 products with 1 Hz of data frequency provided by Archiving, Validation, and Interpretation of Satellite Oceanographic data from February 2016 to June 2023 are used. Jason-3 GDR-F products contain Jason-3 AMR-2 retrieved PWV data, distances of Jason-3 PWV data to land, AMR-2 brightness temperature observations, etc. This work focuses on improving the accuracy of Jason-3 PWV in coastal regions. Therefore, only Jason-3 PWV observations within 50 km of land areas are kept. For each Jason-3 PWV observation, there is a flag to state its surface type, i.e., "land," "near coast," or "open ocean." The Jason-3 PWV data flagged with "land" are removed in this study and only "near coast" and "open ocean" data are kept. In addition, Jason-3 GDR-F products also contain "rain" and "sea ice" flags to indicate if the Jason-3 PWV observations are impacted by rain and sea ice. In this study, we have also removed those Jason-3 PWV data flagged with "rain" or "sea ice."

B. GNSS PWV Data

GNSS is a powerful water vapor monitoring tool that can precisely measure the water vapor under all-weather conditions. GNSS PWV data have the advantages of high accuracy and high temporal resolution, e.g., half an hour or even a few minutes. GNSS PWV observations have, therefore, been widely used as benchmark data to assess the capabilities of other water vapor observing systems [27], [28], [29].

In this study, GNSS PWV data are used as the reference data to train and evaluate the BPNN PWV models we proposed. GNSS PWV data used in this study are all provided by the Nevada Geodetic Laboratory (NGL) [30]. NGL processes GNSS data and provides related water vapor products for over 17 000 GNSS stations distributed globally. According to the evaluation results reported by Ding et al. [31], NGL PWV products have an accuracy of 2.56 kg/m^2 when compared with the radiosonde data from 1994 to 2020.

To estimate the GNSS PWV, NGL processes the GNSS raw data in precise point positioning (PPP) mode [32], [33]. The Zenith tropospheric delay (ZTD) can be estimated as an unknown parameter during the PPP calculation process. Since ZTD can be separated into two parts, i.e., zenith wet delay (ZWD) and Zenith hydrostatic delay (ZHD), ZWD value can then be obtained after removing the ZHD from ZTD

$$\mathrm{ZWD} = \mathrm{ZTD} - \mathrm{ZHD}. \tag{1}$$

For NGL, the ZHD values are obtained by interpolating the Vienna mapping function (VMF1) grid product. Finally, the ZWD values are converted to PWV via the equations proposed by Bevis et al. [5]

$$\mathrm{PWV} = \mathrm{ZWD} \times \mathrm{PWV}_{\mathrm{factor}} \tag{2}$$

$$\mathrm{PWV}_{\mathrm{factor}} = \frac{10^6}{\rho R_v \left(\frac{k_3}{T_m} + k_2 - m k_1\right)} \tag{3}$$

where ρ represents the density of water. k_1 (0.776 K/Pa), k_2 (0.704 K/Pa), and k_3 (3739.0 K/Pa) are three empirical refractivity constants. R_v (461.5 J/K/kg) is the gas constant for water

vapor. m (0.6220) is the ratio between the molar mass of water vapor and molar mass of dry air. T_m is the mean atmospheric temperature in the unit of Kelvin. For NGL, VMF1 interpolated mean atmospheric temperature is used.

Jason-3 PWV and GNSS PWV have different reference heights. Specifically, the reference height of Jason-3 PWV is sea level, while the reference height of GNSS PWV is the height of the GNSS station. In this study, we have adopted an empirical PWV reduction equation proposed by Kouba [34] to reduce the NGL GNSS PWV from the height of GNSS station to sea level (reference height of Jason-3 PWV)

$$\mathrm{PWV}_{\mathrm{sea}} = \mathrm{PWV}_{\mathrm{station}} \times \exp\left(\frac{h_s}{2000}\right) \tag{4}$$

where $\mathrm{PWV}_{\mathrm{sea}}$ represents the reduced PWV at sea level; $\mathrm{PWV}_{\mathrm{station}}$ is the PWV before reduction; h_s is the height of station (unit: m) above or below sea level. Considering that large reduction errors may be introduced from this empirical reduction equation, only those GNSS stations with a height less than 500 m from the sea level (Jason-3 PWV reference height) are selected.

After obtaining the reduced GNSS PWV, we start to generate Jason-3 versus GNSS PWV data pairs. It is well known that water vapor is highly active in both space and time domains. In the previous studies, a relatively relaxed spatial tolerance between altimetric satellite PWV and reference PWV, e.g., 100 km [35], [36], was used to obtain more PWV data pairs and enhance the reliability of statistical results. However, a relaxed distance tolerance will also lead to a large uncertainty in statistical results. As reported by Wu et al. [7], the RMSE value between shipborne GNSS PWV and altimetric satellite PWV increased from 2.29 to 3.32 kg/m^2 when the distance tolerance threshold between GNSS stations and altimetric satellites increased from 50 to 200 km. In this study, to minimize the non-negligible impact caused by the difference in geographical locations between Jason-3 PWV and GNSS PWV, a much stricter distance tolerance, i.e., 20 km, between Jason-3 PWV and GNSS PWV is adopted. In addition, NGL PWV data are provided with a temporal resolution of 5 min. This means that, for each Jason-3 versus GNSS PWV match, the observation time of GNSS PWV and Jason-3 PWV is basically synchronous (temporal discrepancy less than 2.5 min).

After considering all the factors mentioned above, a total of 2076 GNSS stations meet the selection criteria. The distribution of GNSS stations used in this study is displayed in Fig. 1(a). It should be noted that Jason-3 PWV products also provide valid PWV data over continental waters, such as large lakes. The PWV data in inland water areas and inland water-land interface areas are flagged as "open ocean" and "near coast" observations, respectively, in the Jason-3 official products. In this study, all those Jason-3 PWV flagged as "open ocean" or "near coast" are used. This is the reason why some GNSS stations in this study are located near continental waters.

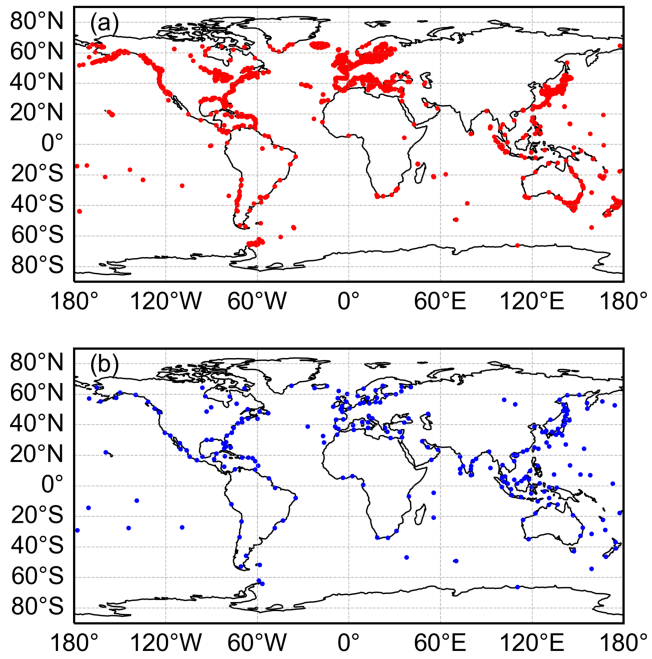

Fig. 1. Distribution of (a) 2076 GNSS stations and (b) 237 radiosonde stations used in this study. GNSS PWV observations are used for BPNN PWV model training and evaluation, while radiosonde PWV observations are only used for model evaluation.

C. Radiosonde PWV Data

Radiosondes are traditional meteorological instruments that can observe a wide variety of meteorological parameters including water vapor at different heights above the Earth surface. In this study, radiosonde observations provided by the Integrated Global Radiosonde Archive (IGRA) [37] are used to evaluate the performances of BPNN models proposed. The radiosonde PWV ($\mathrm{PWV}_{\mathrm{RS}}$) can be calculated by integrating specific humidity with respect to air pressure [38]

$$\mathrm{PWV}_{\mathrm{RS}} = \frac{1}{g}\int_{P_{\mathrm{top}}}^{P_s} q\,dP \tag{5}$$

where g is the gravitational acceleration (9.81 m/s^2). P represents air pressure in unit of Pa. P_s and P_{top} represent the air pressure at the Earth surface and the top of troposphere, respectively. q is the specific humidity (kg/kg), which can be calculated using radiosonde water vapor pressure data

$$q = \frac{0.622e}{P - 0.378e} \tag{6}$$

where e is the water vapor pressure in units of Pa.

Compared with GNSS, the radiosonde has a much sparser spatial distribution and lower temporal resolution. For each IGRA radiosonde station, there is normally only one or two radiosonde profiles per day. To generate enough Jason-3 versus radiosonde PWV matches, the distance and time tolerances for data selection are relaxed to 40 km and 30 min, respectively. It should also be noted, the radiosonde PWV observations used have also been reduced to the sea level (the reference height of Jason-3 PWV) using (4) for the same consideration mentioned before. Finally, Jason-3 versus radiosonde PWV matches are

TABLE I
BPNN MODELS ADOPTED AND THE CORRESPONDING INPUT FEATURES USED FOR MODEL TRAINING

BPNN model	Input parameters used for model training
BPNN-I	• Brightness temperature observations at 18.7, 23.8, and 34 GHz • Distances of Jason-3 footprints to land
BPNN-II	• Jason-3 original PWV from official products • Distances of Jason-3 footprints to land

available only at 237 radiosonde stations. The distribution of radiosonde stations has been shown in Fig. 1(b).

III. DESIGN OF BPNN PWV MODELS

The BPNN model is an effective computational tool that can precisely model the complex nonlinear relationships between different variables [39]. A BPNN model consists of three parts, i.e., an input layer, one or more hidden layers, and an output layer. The hidden layer, between the input layer and the output layer, contains a number of hidden neurons. It is responsible for performing the calculation with the use of data from the input layer. The output layer represents the outcomes calculated based on the inputs.

In this study, two BPNN models, i.e., BPNN-I and BPNN-II, with different combinations of input features are proposed. As shown in Table I, for BPNN-I, Jason-3 AMR-2 brightness temperature observations (at channels 18.7, 23.8, and 34 GHz) and the distances of Jason-3 footprints to land are used as the input features. For BPNN-II, Jason-3 original PWV (PWV from Jason-3 official products) and the distances of Jason-3 footprints to land are applied as model input features. For the output layer, GNSS PWV observations are applied as the reference data to train the models. Specifically, Jason-3 data and GNSS PWV data in the years 2016 and 2017 are used for model training. In total, there are 215781 training samples used. GNSS and radiosonde PWV observations from January 2018 to June 2023 are used to test the performances of the two models proposed.

The numbers of hidden layers and neurons considerably impact the computation accuracy and the time complexity. However, currently, there is no definitive rule to determine the number of hidden layers and hidden neurons. The excessive hidden layers and neurons may lead to a massive amount of computation time and the overfitting problem [40], [41]. To determine the optimal numbers of hidden layers and neurons, based on the training data in 2016 and 2017, we have conducted the five-fold cross-validation for two BPNN models with different numbers of hidden layers (from 1 layer to 3 layers) and neurons (4, 8, 16, and 32 neurons). For each five-fold cross-validation, we randomly divide the training data in 2016 and 2017 into five equal subsets. Then, we train the model on four of the five subsets, while the remaining one subset is utilized to validate the model's performance. We repeat this process five times with each subset serving as the validation subset once. Therefore, for each five-fold cross-validation, we can get five PWV RMSE values for each BPNN model. Finally, the average of five BPNN PWV RMSE values is used as the overall metric for the five-fold cross-validation. As shown in Table II, for each hidden layer and neuron combination, we have calculated the average RMSE based on the five-fold cross-validation method. According to the numerical validation results shown in Table II, for BPNN-I, three hidden layers are adopted with each layer consisting of 16 neurons. BPNN-II model is designed with two hidden layers. Each hidden layer in BPNN-II contains eight neurons. In addition, the hyperbolic tangent sigmoid transfer function and pure linear activation equation are selected as the activation functions for the hidden layer and output layer, respectively.

TABLE II
AVERAGE RMSE VALUES OF BPNN PWV (UNIT: KG/M^2) BASED ON THE FIVE-FOLD CROSS-VALIDATION METHOD FOR DIFFERENT NUMBERS OF HIDDEN LAYERS AND NEURONS

Number of neurons for each hidden layer	RMSE of BPNN-I PWV (kg/m^2)			RMSE of BPNN-II PWV (kg/m^2)		
	1 hidden layer	2 hidden layers	3 hidden layers	1 hidden layer	2 hidden layers	3 hidden layers
4 neurons	3.06	2.45	2.31	2.95	2.59	2.50
8 neurons	2.54	2.05	2.08	2.55	2.37	2.38
16 neurons	2.21	2.00	1.96	2.41	2.39	2.39
32 neurons	2.12	2.12	2.03	2.40	2.44	2.40

IV. RESULTS AND ANALYSES

A. Overall Performances of BPNN PWV Models With Respect to the Distance to Land

The accuracies of BPNN-enhanced Jason-3 PWV with respect to different distances to land are evaluated by GNSS and radiosonde PWV. All Jason-3/BPNN PWV within 50 km of land are classified into 10 categories according to their distances to land (from 0 to 50 km with an even interval of 5 km). There are 328626, 171757, 93610, 35999, and 2921 Jason-3/BPNN versus GNSS PWV matches, respectively, located at the distance categories of 0 to 5 km, 5 to 10 km, 10 to 15 km, 15 to 20 km, and 20 to 25 km. For the distance from 25 to 50 km, totally 5975 Jason-3/BPNN versus GNSS PWV matches are used for evaluation.

The corresponding statistical results of BPNN PWV evaluated by GNSS PWV for different distance categories from 0 to 50 km are shown in Fig. 2. We can obviously find that, contaminated by land, the accuracy of Jason-3 original PWV degrades rapidly in the coastal areas. The RMSE and mean absolute error (MAE) of Jason-3 original PWV all increase considerably when the distance of Jason-3 footprint to land reduces to less than 25 km. Specifically, the average RMSE of Jason-3 original PWV for 0 to 25 km of land is 4.2 kg/m^2, while the corresponding average RMSE for 25–50 km of land is 1.3 kg/m^2. This means that, affected by the land, the accuracy of Jason-3 original PWV is degraded by 223%.

Both RMSE and MAE statistical results show that PWV from two BPNN models have a better accuracy than Jason-3 original PWV in the coastal areas (within 25 km of land). Specifically, the average PWV RMSE values of BPNN-I and BPNN-II in the coastal areas are 2.7 and 3.2 kg/m^2, respectively, which correspond to RMSE reductions (accuracy improvements) of 35.7% and 23.8%, respectively, compared with Jason-3 original PWV. In addition, the average MAE value of Jason-3 original PWV in the coastal areas is 3.1 kg/m^2. After applying BPNN-I

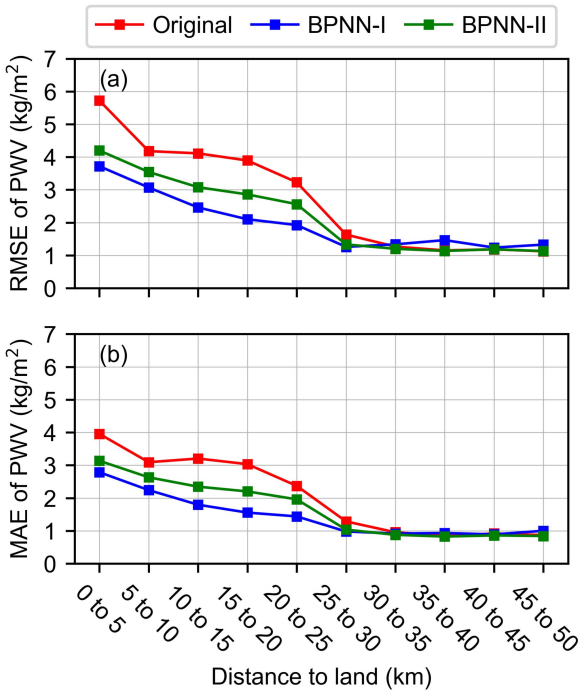

Fig. 2. (a) RMSE and (b) MAE of Jason-3 original PWV and BPNN PWV evaluated by GNSS PWV for different distances (0 to 50 km) from Jason-3 footprints to land areas.

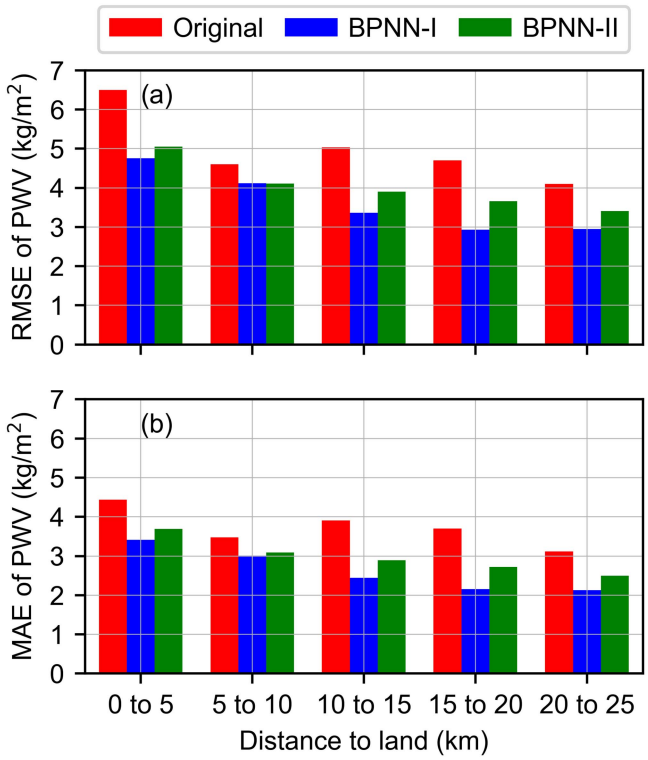

Fig. 3. (a) RMSE and (b) MAE of Jason-3 original PWV and BPNN PWV evaluated by radiosonde PWV for different distances from Jason-3 footprints to land areas.

and BPNN-II, the average MAE value in the coastal areas is reduced to 2.0 and 2.5 kg/m^2, respectively. BPNN-I outperforms BPNN-II for coastal areas. The possible reason could be that, compared to brightness temperature data, Jason-3 original PWV data have greater uncertainties due to the introduction of retrieval errors from Jason-3 PWV official retrieval algorithms. When the distances of Jason-3 radar footprints to land areas are more than 25 km, the impact of land contamination on Jason-3 is insignificant. The PWV output by the two BPNN models has a similar quality to the Jason-3 original PWV.

The overall performances of BPNN models evaluated by the radiosonde PWV have been shown in Fig. 3. In this study, for the distance categories of 0 to 5 km, 5 to 10 km, 10 to 15 km, 15 to 20 km, and 20 to 25 km, 5175, 3441, 2391, 1919, and 1438 Jason-3/BPNN versus radiosonde PWV matches are used for evaluation, respectively. However, the number of Jason-3/BPNN versus radiosonde PWV matches is very limited for the areas >25 km of land. Particularly for distance categories of 40–45 km and 45–50 km, there are only 31 and 14 matches, respectively. Considering: 1) the number of Jason-3/BPNN versus radiosonde matches in the areas >25 km of land is insufficient; 2) the Jason-3 original PWV observations are generally free of land contamination when Jason-3 is more than 25 km away from land areas, in this study, only the radiosonde evaluation results for the distances from 0 to 25 km are presented.

The numerical results evaluated by radiosonde PWV evidently reveal that PWV estimated by two BPNN models have a higher accuracy than Jason-3 original PWV. The average RMSE of Jason-3 original PWV evaluated by radiosonde PWV in coastal areas is 5.0 kg/m^2, while the average RMSE values of BPNN-I and BPNN-II models are 3.6 kg/m^2 (28.0% of RMSE reduction) and 4.0 kg/m^2 (20.0% of RMSE reduction), respectively. In addition, the average MAE value of Jason-3 original PWV evaluated by radiosonde in the coastal areas is 3.7 kg/m^2. For BPNN-I and BPNN-II models, the average PWV MAE values are reduced to 2.6 and 3.0 kg/m^2, respectively.

Given that the BPNN models are only effective for areas within 25 km of land, in the following analyses, we only focus on analyzing the performances of the BPNN PWV models in the coastal areas (within 25 km of land). In addition, radiosonde PWV data are only used for the overall evaluation of BPNN models in this section and have not been used for Sections IV-B to IV-F since the number of Jason-3/BPNN versus radiosonde PWV matches is not sufficient to support detailed analyses.

B. *Time Series of BPNN PWV Accuracy*

The performances of BPNN models in the time domain are analyzed. Only Jason-3/BPNN versus GNSS PWV data pairs within 25 km from the coast are used. As we mentioned in Section IV-A, most of Jason-3/BPNN versus GNSS PWV data pairs are located within 10 km of land. This implies the RMSE statistical results will be mainly determined by those BPNN versus GNSS PWV data pairs within 10 km of land. To better show the performances of the BPNN PWV models, we first compute the RMSE of BPNN PWV for each 5-km distance category from 0 to 25 km. Then, the average of RMSE values for these five distance categories is used as the overall RMSE for the coastal area (within 25 km of land). This RMSE calculation strategy has

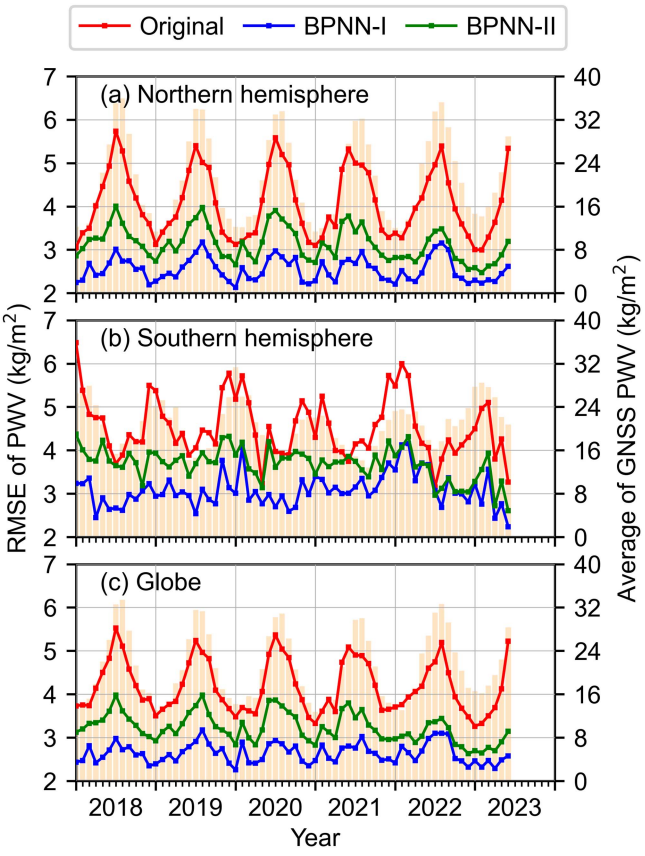

Fig. 4. RMSE of Jason-3 original PWV and BPNN PWV evaluated by GNSS PWV in (a) the northern hemisphere, (b) the southern hemisphere, and (c) the globe, for each month during the period of January 2018–June 2023. The bars represent the monthly average values of GNSS PWV. Only Jason-3/BPNN PWV values within 25 km of land are used.

also been used in the following sections, i.e., Sections IV-B to IV-F.

The BPNN PWV monthly RMSE values assessed by GNSS PWV for the northern hemisphere, the southern hemisphere, and the globe in the entire evaluation period (January 2018 to June 2023) are displayed in Fig. 4(a), (b), and (c), respectively. The monthly mean GNSS PWV values during the evaluation period are also shown in Fig. 4. The RMSE values of both Jason-3 original PWV and BPNN PWV evidently show a seasonal variation pattern in the northern hemisphere. However, the seasonal pattern is less obvious in the southern hemisphere for BPNN models. In addition, we can find that the global pattern of PWV RMSE variation is basically consistent with that of the northern hemisphere. This is because, in this study, the number of GNSS observations used for evaluation in the northern hemisphere (552039 evaluation samples) is much more than that in the southern hemisphere (86849 evaluation samples). It is expected that the global statistical results will be mainly dominated by the data in the northern hemisphere.

The PWV RMSE values are closely associated with the magnitude of PWV values. For all months, BPNN PWV evidently shows a better accuracy than the original PWV, particularly for the months with large water vapor magnitudes. The results in Fig. 4 show that all BPNN models are still effective for the years of 2022 and 2023 although the BPNN models are trained using data of 2016 and 2017. We have also conducted the annual RMSE statistics for BPNN PWV from 2018 to 2022. The performances of the BPNN models remain stable after model training as the global water vapor conditions during the whole experimental period changed insignificantly [42]. Compared with Jason-3 original PWV, the RMSE values of BPNN-I PWV are reduced by 40.1%, 36.7%, 38.2%, 37.0%, and 34.4%, for 2018, 2019, 2020, 2021, and 2022, respectively. BPNN-II model has smaller RMSE reductions than the BPNN-I model. The annual PWV reductions are 22.7%, 21.0%, 21.7%, 22.5%, and 26.8%, respectively, from 2018 to 2022. The annual RMSE for 2023 has not been calculated because of the incompleteness of data. For the year 2023, only the Jason-3 PWV data from January to June are used in this study.

C. *Performances of BPNN Models for Different Water Vapor Conditions*

Fig. 4 shows that in wet months, the BPNN models have reduced the PWV RMSE much more than in dry months. To better understand the performances of BPNN models under different water vapor conditions, we have divided the entire evaluation period (January 2018–June 2023) into three groups, i.e., wet months, dry months, and normal months, based on the absolute values of monthly average GNSS PWV as shown in Fig. 4

1) Wet months: June to September for the northern hemisphere; December and January to March for the southern hemisphere.
2) Dry months: December and January to March for the northern hemisphere; June to September for the southern hemisphere.
3) Normal months: other months except for wet months and dry months.

The accuracy statistics of Jason-3 original PWV and BPNN PWV in three groups of months are shown in Table III. Only Jason-3 PWV within 25 km of land areas are used. We can find the RMSE values for wet months are much larger than those for dry months. Specifically, for wet months, the Jason-3 original PWV RMSE values are 5.1, 5.2, and 5.1 kg/m^2, respectively, for the northern hemisphere, the southern hemisphere, and the globe. In dry months, the RMSE values of Jason-3 original PWV are 3.3, 4.1, and 3.4 kg/m^2, respectively, for the northern hemisphere, the southern hemisphere, and the globe.

After applying the BPNN models, we can clearly see that the Jason-3 PWV RMSE values have reduced for all three groups of months. BPNN-I achieves a better performance than BPNN-II for all month categories. Particularly for the wet months, BPNN-I model reduces the PWV RMSE by 43.1%, 34.6%, and 41.2%, respectively, for the northern hemisphere, the southern hemisphere, and the globe. The accuracy improvements for dry months and normal months are also significant but smaller than for wet months. For dry months, the Jason-3 PWV accuracy improvements (RMSE reductions) benefitting from two BPNN models can be up to 30.3%, 26.8%, and 29.4%, respectively, for the northern hemisphere, the southern hemisphere, and the

TABLE III
AVERAGE OF GNSS PWV AND AVERAGE RMSE OF JASON-3 PWV WITHIN 25 KM OF LAND FOR THREE GROUPS OF MONTHS, I.E., WET MONTHS, DRY MONTHS, AND NORMAL MONTHS, IN THE NORTHERN HEMISPHERE, THE SOUTHERN HEMISPHERE, AND THE GLOBE

Hemisphere	Month	Average of GNSS PWV (kg/m^2)	Average RMSE of Jason-3 original PWV (kg/m^2)	Average RMSE of BPNN PWV (kg/m^2)	
				BPNN-I	BPNN-II
Northern hemisphere	Wet	31.1	5.1	2.9 (-43.1%)	3.6 (-29.4%)
	Dry	13.2	3.3	2.3 (-30.3%)	2.9 (-12.1%)
	Normal	19.5	4.0	2.4 (-40.0%)	3.0 (-25.0%)
Southern hemisphere	Wet	25.1	5.2	3.4 (-34.6%)	3.8 (-26.9%)
	Dry	16.5	4.1	3.0 (-26.8%)	3.6 (-12.2%)
	Normal	20.5	4.5	3.1 (-31.1%)	3.7 (-17.8%)
Globe	Wet	30.3	5.1	3.0 (-41.2%)	3.6 (-29.4%)
	Dry	13.7	3.4	2.4 (-29.4%)	3.0 (-11.8%)
	Normal	19.7	4.0	2.6 (-35.0%)	3.2 (-20.0%)

The reduction of BPNN PWV RMSE in percentage with respect to Jason-3 original PWV have been shown in the parentheses.

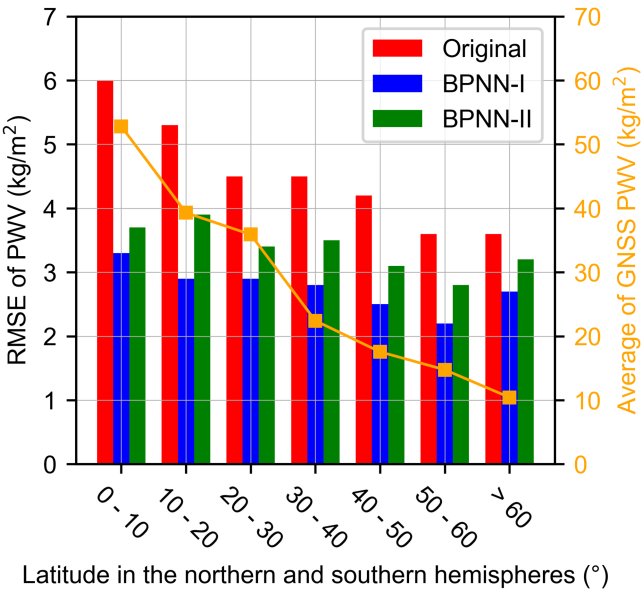

Fig. 5. Average RMSE of Jason-3 original PWV and BPNN PWV for the coastal areas (within 25 km of land) at different latitudes. The orange line represents the average values of GNSS PWV for different latitude categories.

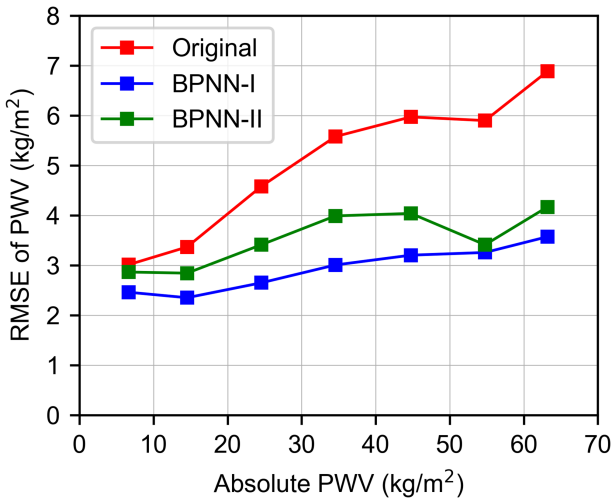

Fig. 6. RMSE of Jason-3 original PWV and BPNN PWV evaluated by GNSS PWV under different magnitudes of absolute PWV (average of GNSS PWV) for coastal areas (within 25 km of land).

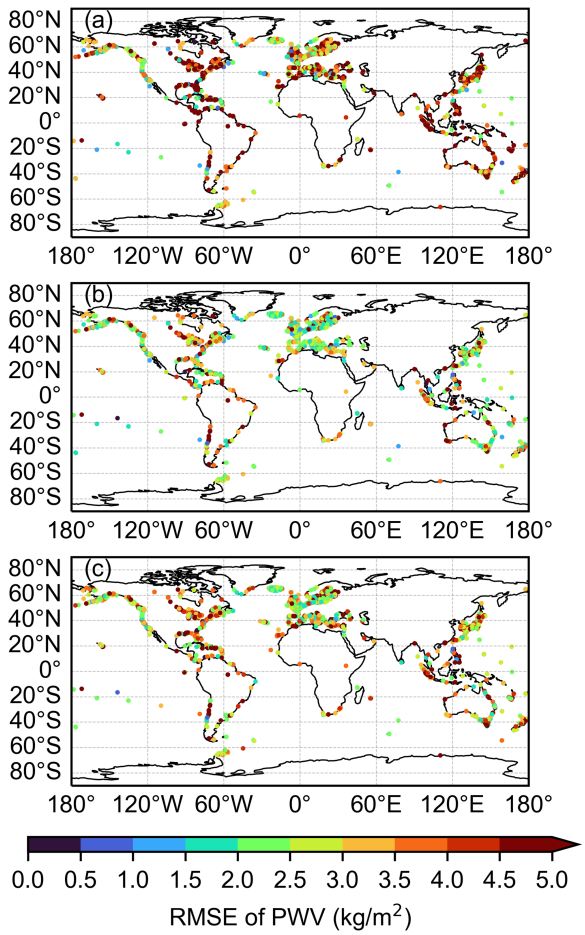

Fig. 7. RMSE of (a) Jason-3 original PWV, (b) BPNN-I PWV, and (c) BPNN-II PWV, evaluated by GNSS PWV for coastal areas (within 25 km of land) at each of the 2010 GNSS stations.

globe. For normal months, the PWV accuracy improvements in coastal areas for the northern hemisphere, the southern hemisphere, and the globe can reach 40.0%, 31.1%, and 35.0%, respectively.

The RMSE values of Jason-3 original PWV and BPNN models in the southern hemisphere are larger than those in the northern hemisphere. This could be caused by the different evaluation samples used for the two hemispheres. For the dry

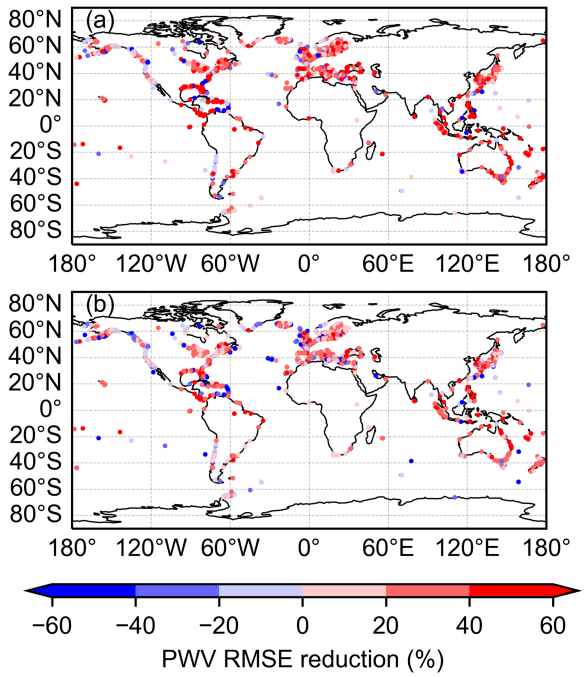

Fig. 8. PWV RMSE reduction of (a) BPNN-I model and (b) BPNN-II model for coastal areas (within 25 km of land) evaluated by GNSS PWV at each of the 2010 GNSS stations, compared to Jason-3 original PWV.

and normal months, we can see that the absolute PWV values (the average of GNSS PWV) used for evaluation in the southern hemisphere are higher than those in the northern hemisphere. For the wet months, we can see that the absolute PWV value (average of GNSS PWV) in the northern hemisphere is larger than that in the southern hemisphere. But the RMSE values of original PWV and BPNN PWV in the southern hemisphere are larger than those in the northern hemisphere in both dry and normal months and wet months. This could be caused by the limited number of evaluation samples for the southern hemisphere.

D. Performances of BPNN Models at Different Latitudes

To investigate the performances of the BPNN PWV models at different latitude regions, we have divided the Jason-3/BPNN versus GNSS PWV data pairs located within 25 km of land into seven categories based on their latitudes, i.e., latitude 0°–60° with an interval of 10°, and >60°, for both the northern and southern hemispheres. The RMSE values of Jason-3 original PWV and BPNN PWV assessed by GNSS PWV at different latitude categories have been calculated and shown in Fig. 5. The corresponding GNSS mean PWV values at different latitudes are also shown in this figure. We can find a decreasing trend in the PWV absolute value from 52.8 to 10.4 kg/m^2 when the latitude increases from 0° to above 60°. Correspondingly, the Jason-3 PWV RMSE generally shows a decreasing trend with the increase of latitude from 0° to 60°. The PWV from two BPNN models shows a better accuracy than Jason-3 original PWV for all latitude categories. In the latitude interval of 0° to 10°, evaluated by GNSS PWV, the Jason-3 original PWV data have a RMSE value of 6.0 kg/m^2, while the PWV RMSE values of BPNN-I and BPNN-II models are 3.3 kg/m^2 (45.0% of RMSE reduction) and 3.7 kg/m^2 (38.3% of RMSE reduction), respectively. When the latitude increases to above 60°, the RMSE value of Jason-3 original PWV decreases to 3.6 kg/m^2. The corresponding PWV RMSE values for BPNN-I and BPNN-II models are decreased to 2.7 kg/m^2 (25.0% of RMSE reduction) and 3.2 kg/m^2 (11.1% of RMSE reduction), respectively.

E. Performances of BPNN Models With Respect to the Absolute PWV Value

The evaluation results in Sections IV-B to IV-D show that the accuracies of BPNN PWV are closely associated with the absolute water vapor amount. Therefore, in this section, we explore the performances of BPNN PWV models corresponding to different magnitudes of PWV. We divide all Jason-3/BPNN versus GNSS PWV data pairs in coastal areas (within 25 km of land) during the whole evaluation period into seven groups according to the magnitude of GNSS PWV, i.e., 0 to 70 kg/m^2 with an interval of 10 kg/m^2 (0–10 kg/m^2, 10–20 kg/m^2, 20–30 kg/m^2, and etc). We have not conducted the statistics for those Jason-3/BPNN versus GNSS PWV data pairs with a magnitude larger than 70 kg/m^2 due to the small number of samples. Then, we calculate the average RMSE of BPNN PWV within 25 km of land for each group. The average of GNSS PWV for each PWV group is also calculated. Finally, a function of BPNN PWV RMSE with respect to PWV magnitude is shown in Fig. 6. We can clearly see that both Jason-3 original PWV RMSE and BPNN PWV RMSE increase with the increase of absolute PWV. Specifically, when the magnitude of the PWV increases from 6.7 to 63.2 kg/m^2, the RMSE of Jason-3 original PWV increases from 3.0 to 6.9 kg/m^2 (0.069 of average RMSE increasing rate).

For BPNN models, the PWV RMSE values increase at a relatively slower rate. For absolute PWV of 0–10 kg/m^2, the PWV RMSE values of BPNN-I and BPNN-II models are 2.5 and 2.9 kg/m^2, respectively. For absolute PWV of 60–70 kg/m^2, the RMSE values of BPNN-I and BPNN-II arrive at 3.6 and 4.2 kg/m^2, respectively.

Our numerical results in Sections IV-B to IV-E show that, examined by GNSS PWV, BPNN models have a larger PWV RMSE value when the absolute PWV is higher. One potential reason is that the uncertainty of GNSS PWV used for evaluation increases as weather conditions become wetter. Another potential reason is that brightness temperature observations also have larger uncertainties under wetter weather conditions. This further degrades the accuracies of BPNN models' PWV outputs.

Based on the PWV RMSE values and the absolute PWV values shown in Fig. 6, we can calculate the corresponding relative RMSE (the ratio of BPNN PWV RMSE to the average of GNSS PWV value) for different categories of absolute PWV. Specifically, the relative RMSE of Jason-3 original PWV is 44.8% for the 0–10 kg/m^2 category. The corresponding relative RMSE values of BPNN-I and BPNN-II are 37.3% and 43.3%, respectively. When the absolute PWV value increases from 60 to 70 kg/m^2, the relative RMSE values of Jason-3 original PWV,

BPNN-I PWV, and BPNN-II PWV are 10.9%, 5.7%, and 6.6%, respectively.

F. Station-Based BPNN PWV Accuracy

The RMSE values of Jason-3 original PWV and BPNN PWV at each GNSS station during the entire evaluation period (January 2018 to June 2023) are presented in Fig. 7. A total of 2010 GNSS stations have Jason-3/BPNN versus GNSS PWV pairs within 25 km of land. It should be noted that this number is different from 2076 GNSS stations, which have PWV pairs within 50 km of coastline during the period of February 2016–June 2023. For Jason-3 original PWV, 1043 out of the total 2010 GNSS stations have PWV RMSE values exceeding 4 kg/m^2. After applying BPNN-I and BPNN-II models, there are only 324 and 588 stations, respectively, with a PWV RMSE above 4 kg/m^2.

The corresponding station-wise RMSE reduction of BPNN PWV compared to Jason-3 original PWV at each GNSS station has been shown in Fig. 8. BPNN-I and BPNN-II models enhance the PWV accuracy at 1657 and 1578 GNSS stations, respectively. In addition, with the use of BPNN-I and BPNN-II models, there are 1310 and 1129 GNSS stations, respectively, with over 20% of PWV RMSE reduction.

V. Conclusion

The accuracy of Jason-3 PWV products degrades significantly in coastal sea–land interface areas. By using GNSS PWV as the reference values, we have trained two BPNN PWV models with different combinations of input variables, i.e., BPNN-I model (input parameters: Jason-3 AMR-2 brightness temperature observations (at 18.7, 23.8, and 34 GHz) and the distance of Jason-3 to land) and BPNN-II model (input parameters: Jason-3 original PWV and the distance of Jason-3 to land), to enhance the accuracy of Jason-3 PWV products in global coastal areas. Two-year (2016 and 2017) Jason-3 and GNSS data are used to train the BPNN models. More than 5-year (from January 2018 to June 2023) GNSS and radiosonde PWV data are used for model testing.

Our results show that two BPNN PWV models considerably improve the accuracy of Jason-3 PWV for the coastal areas (within 25 km of land). BPNN-I model outperforms BPNN-II model. Evaluated by GNSS PWV, the RMSE of Jason-3 original PWV in the coastal areas is 4.2 kg/m^2. Using the proposed BPNN-I and BPNN-II models, the RMSE values are reduced to 2.7 kg/m^2 (35.7% of RMSE reduction) and 3.2 kg/m^2 (23.8% of RMSE reduction), respectively. Correspondingly, evaluated by radiosonde PWV data, the RMSE of Jason-3 original PWV in the coastal areas is 5.0 kg/m^2, while the RMSE values of BPNN-1 and BPNN-II are 3.6 kg/m^2 (28.0% of RMSE reduction) and 4.0 kg/m^2 (20.0% of RMSE reduction), respectively.

The performances of the BPNN models remained stable over the evaluation years. We can still find considerable accuracy improvements in Jason-3 PWV for the year of 2022 (the fifth year after the model training). Specifically, the Jason-3 PWV accuracy improvements benefitting from BPNN models in the coastal areas can be up to 40.1%, 36.7%, 38.2%, 37.0%, and 34.4%, respectively, for 2018, 2019, 2020, 2021, and 2022.

Overall, the results of this study have demonstrated the effectiveness of the BPNN PWV models proposed. For other altimetric satellite missions, users may also be able to establish the BPNN PWV models by using GNSS PWV observations and corresponding altimetric satellites' observational data over coastal areas. More accurate altimetric satellite water vapor data in coastal areas are expected after applying the well-trained BPNN models. Exploring and validating the performances of BPNN PWV models for other altimetric satellites over coastal areas could be one potential work in the future.

Acknowledgment

The authors acknowledge the Nevada Geodetic Laboratory (NGL) for providing GNSS PWV data. The NGL PWV data can be downloaded via http://geodesy.unr.edu/gps_timeseries/trop/. We also thank AVISO (Archiving, Validation, and Interpretation of Satellite Oceanographic data) for providing Jason-3 products (http://aviso.altimetry.fr). We thank NOAA National Centers for Environmental Information for providing IGRA radiosonde data version 2 (ftp.ncei.noaa.gov/pub/data/igra/).

References

[1] M. J. Fernandes, C. Lázaro, M. Ablain, and N. Pires, "Improved wet path delays for all ESA and reference altimetric missions," *Remote Sens. Environ.*, vol. 169, pp. 50–74, 2015, doi: 10.1016/j.rse.2015.07.023.

[2] J. G. Marsh, "Satellite altimetry," *Rev. Geophys.*, vol. 21, no. 3, pp. 574–580, 1983, doi: 10.1029/RG021i003p00574.

[3] S. Vignudelli et al., "Satellite altimetry measurements of sea level in the coastal zone," *Surv. Geophys.*, vol. 40, pp. 1319–1349, 2019, doi: 10.1007/s10712-019-09569-1.

[4] J. Benveniste et al., "Coastal sea level anomalies and associated trends from Jason satellite altimetry over 2002–2018," *Sci. Data*, vol. 7, no. 1, 2020, Art. no. 357, doi: 10.1038/s41597-020-00694-w.

[5] M. Bevis et al., "GPS meteorology: Mapping zenith wet delays onto precipitable water," *J. Appl. Meteorol. Climatol.*, vol. 33, no. 3, pp. 379–386, 1994.

[6] M. J. Fernandes, C. Lázaro, and T. Vieira, "On the role of the troposphere in satellite altimetry," *Remote Sens. Environ.*, vol. 252, 2021, Art. no. 112149, doi: 10.1016/j.rse.2020.112149.

[7] Z. Wu et al., "Evaluation of Shipborne GNSS precipitable water vapor over global oceans from 2014 to 2018," *IEEE Trans. Geosci. Remote Sens.*, vol. 60, 2022, Art. no. 5802515, doi: 10.1109/TGRS.2022.3142745.

[8] S. Brown, "A novel near-land radiometer wet path-delay retrieval algorithm: Application to the Jason-2/OSTM advanced microwave radiometer," *IEEE Trans. Geosci. Remote Sens.*, vol. 48, no. 4, pp. 1986–1992, Apr. 2010, doi: 10.1109/TGRS.2009.2037220.

[9] T. Vieira, M. J. Fernandes, and C. Lazaro, "Independent assessment of on-board microwave radiometer measurements in coastal zones using tropospheric delays from GNSS," *IEEE Trans. Geosci. Remote Sens.*, vol. 57, no. 3, pp. 1804–1816, Mar. 2018, doi: 10.1109/TGRS.2018.2869258.

[10] P. Aguiar, T. Vieira, C. Lázaro, and M. J. Fernandes, "An improved altimetry wet tropospheric correction retrieval over coastal regions for the Sentinel-3 mission," *IEEE J. Sel. Topics Appl. Earth Observ. Remote Sens.*, vol. 16, pp. 7979–7991, 2023, doi: 10.1109/JSTARS.2023.3308721.

[11] S. Thao, L. Eymard, E. Obligis, and B. Picard, "Comparison of regression algorithms for the retrieval of the wet tropospheric path," *IEEE J. Sel. Topics Appl. Earth Observ. Remote Sens.*, vol. 8, no. 9, pp. 4302–4314, Sep. 2015, doi: 10.1109/JSTARS.2015.2442416.

[12] T. Vieira, M. J. Fernandes, and C. Lázaro, "An enhanced retrieval of the wet tropospheric correction for Sentinel-3 using dynamic inputs from ERA5," *J. Geodesy*, vol. 96, no. 4, 2022, Art. no. 28, doi: 10.1007/s00190-022-01622-z.

[13] E. Obligis, L. Eymard, N. Tran, S. Labroue, and P. Femenias, "First three years of the microwave radiometer aboard Envisat: In-flight calibration, processing, and validation of the geophysical products," *J. Atmos. Ocean. Technol.*, vol. 23, no. 6, pp. 802–814, 2006, doi: 10.1175/JTECH1878.1.

[14] E. Obligis, A. Rahmani, L. Eymard, S. Labroue, and E. Bronner, "An improved retrieval algorithm for water vapor retrieval: Application to the envisat microwave radiometer," *IEEE Trans. Geosci. Remote Sens.*, vol. 47, no. 9, pp. 3057–3064, Sep. 2009, doi: 10.1109/TGRS.2009.2020433.
[15] I. M. Held and B. J. Soden, "Water vapor feedback and global warming," *Annu. Rev. Energy Environ.*, vol. 25, no. 1, pp. 441–475, 2000, doi: 10.1146/annurev.energy.25.1.441.
[16] J. He and Z. Liu, "Water vapor retrieval from MODIS NIR channels using ground-based GPS data," *IEEE Trans. Geosci. Remote Sens.*, vol. 58, no. 5, pp. 3726–3737, May 2020, doi: 10.1109/TGRS.2019.2962057.
[17] J. He and Z. Liu, "Refining MODIS NIR atmospheric water vapor retrieval algorithm using GPS-derived water vapor data," *IEEE Trans. Geosci. Remote Sens.*, vol. 59, no. 5, pp. 3682–3694, May 2021, doi: 10.1109/TGRS.2020.3016655.
[18] Z. Xiong, X. Sun, J. Sang, and X. Wei, "Modify the accuracy of MODIS PWV in China: A performance comparison using random forest, generalized regression neural network and back-propagation neural network," *Remote Sens.*, vol. 13, no. 11, 2021, Art. no. 2215, doi: 10.3390/rs13112215.
[19] J. Xu and Z. Liu, "A back propagation neural network-based calibration approach for sentinel-3 OLCI near-infrared water vapor product," *IEEE Geosci. Remote Sens. Lett.*, vol. 20, 2023, Art. no. 1000105, doi: 10.1109/LGRS.2023.3235983.
[20] J. Xu and Z. Liu, "Improving the accuracy of MODIS near-infrared water vapor product under all weather conditions based on machine learning considering multiple dependence parameters," *IEEE Trans. Geosci. Remote Sens.*, vol. 61, 2023, Art. no. 4101115, doi: 10.1109/TGRS.2023.3252024.
[21] X. Ma, Y. Yao, B. Zhang, and Z. Du, "FY-3A/MERSI precipitable water vapor reconstruction and calibration using multi-source observation data based on a generalized regression neural network," *Atmos. Res.*, vol. 265, 2022, Art. no. 105893, doi: 10.1016/j.atmosres.2021.105893.
[22] D. Zhu, K. Zhang, L. Yang, S. Wu, and L. Li, "Evaluation and calibration of MODIS near-infrared precipitable water vapor over China using GNSS observations and ERA-5 reanalysis dataset," *Remote Sens.*, vol. 13, no. 14, 2021, Art. no. 2761, doi: 10.3390/rs13142761.
[23] J. Xu and Z. Liu, "Enhanced all-weather precipitable water vapor retrieval from MODIS near-infrared bands using machine learning," *Int. J. Appl. Earth Observ. Geoinf.*, vol. 114, 2022, Art. no. 103050, doi: 10.1016/j.jag.2022.103050.
[24] X. Ma, Y. Yao, B. Zhang, Y. Qin, Q. Zhang, and H. Zhu, "An improved MODIS NIR PWV retrieval algorithm based on an artificial neural network considering the land-cover types," *IEEE Trans. Geosci. Remote Sens.*, vol. 60, 2022, Art. no. 5622412.
[25] L. Zawadzki and M. Ablain, "Accuracy of the mean sea level continuous record with future altimetric missions: Jason-3 vs. Sentinel-3a," *Ocean Sci.*, vol. 12, no. 1, pp. 9–18, 2016, doi: 10.5194/os-12-9-2016.
[26] F. Maiwald et al., "Reliable and stable radiometers for Jason-3," *IEEE J. Sel. Topics Appl. Earth Observ. Remote Sens.*, vol. 9, no. 6, pp. 2754–2762, Jun. 2016, doi: 10.1109/JSTARS.2016.2535281.
[27] L. Huang et al., "High-precision GNSS PWV retrieval using dense GNSS sites and in-situ meteorological observations for the evaluation of MERRA-2 and ERA5 reanalysis products over China," *Atmos. Res.*, vol. 276, 2022, Art. no. 106247, doi: 10.1016/j.atmosres.2022.106247.
[28] Y. Gong, Z. Liu, and J. H. Foster, "Evaluating the accuracy of satellite-based microwave radiometer PWV products using shipborne GNSS observations across the Pacific Ocean," *IEEE Trans. Geosci. Remote Sens.*, vol. 60, 2022, Art. no. 5802210, doi: 10.1109/TGRS.2021.3129001.
[29] L. Huang et al., "Evaluation of hourly PWV products derived from ERA5 and MERRA-2 over the Tibetan Plateau using ground-based GNSS observations by two enhanced models," *Earth Space Sci.*, vol. 8, no. 5, 2021, Art. no. e2020EA001516, doi: 10.1029/2020EA001516.
[30] G. Blewitt et al., "Harnessing the GPS data explosion for interdisciplinary science," *Eos Trans. Amer. Geophysical*, vol. 99, 2018, Art. no. e2020943118, doi: 10.1029/2018EO104623.
[31] J. Ding, J. Chen, W. Tang, and Z. Song, "Spatial–temporal variability of global GNSS-derived precipitable water vapor (1994–2020) and climate implications," *Remote Sens.*, vol. 14, no. 14, 2022, Art. no. 3493, doi: 10.3390/rs14143493.
[32] J. Zumberge, M. Heflin, D. Jefferson, M. Watkins, and F. Webb, "Precise point positioning for the efficient and robust analysis of GPS data from large networks," *J. Geophys. Res. Solid Earth*, vol. 102, no. B3, pp. 5005–5017, 1997, doi: 10.1029/96JB03860.
[33] J. Kouba and P. Héroux, "Precise point positioning using IGS orbit and clock products," *GPS Solution*, vol. 5, no. 2, pp. 12–28, 2001.
[34] J. Kouba, "Implementation and testing of the gridded Vienna mapping function 1 (VMF1)," *J. Geodesy*, vol. 82, no. 4, pp. 193–205, 2008.
[35] Y. Gong and Z. Liu, "Evaluating the accuracy of Jason-3 water vapor product using PWV data from global radiosonde and GNSS stations," *IEEE Trans. Geosci. Remote Sens.*, vol. 59, no. 5, pp. 4008–4017, May 2021, doi: 10.1109/TGRS.2020.3017761.
[36] Z. Wu et al., "Validating HY-2A CMR precipitable water vapor using ground-based and shipborne GNSS observations," *Atmos. Meas. Techn.*, vol. 13, no. 9, pp. 4963–4972, 2020, doi: 10.5194/amt-13-4963-2020.
[37] I. Durre, X. Yin, R. S. Vose, S. Applequist, and J. Arnfield, "Enhancing the data coverage in the integrated global radiosonde archive," *J. Atmos. Ocean. Technol.*, vol. 35, no. 9, pp. 1753–1770, 2018, doi: 10.1175/JTECH-D-17-0223.1.
[38] R. J. Ross and W. P. Elliott, "Tropospheric water vapor climatology and trends over North America: 1973–93," *J. Climate*, vol. 9, no. 12, pp. 3561–3574, 1996, doi: 10.1175/1520-0442(1996)009<3561:TWVCAT>2.0.CO;2.
[39] D. E. Rumelhart, G. E. Hinton, and R. J. Williams, "Learning representations by back-propagating errors," *Nature*, vol. 323, no. 6088, pp. 533–536, 1986.
[40] K. G. Sheela et al., "Review on methods to fix number of hidden neurons in neural networks," *Math. Problems Eng.*, vol. 2013, 2013, Art. no. 425740, doi: 10.1155/2013/425740.
[41] M. Uzair and N. Jamil, "Effects of hidden layers on the efficiency of neural networks," in *Proc. IEEE 23rd Int. Multitopic Conf.*, 2020, pp. 1–6, doi: 10.1109/INMIC50486.2020.9318195.
[42] T. Vieira, P. Aguiar, C. Lázaro, B. Vasconcellos, and M. J. Fernandes, "Impact analysis of global warming on Wet Path Delay over the satellite altimetry era (1993-2022)," *IEEE Trans. Geosci. Remote Sens.*, vol. 62, 2024, Art. no. 5301207, doi: 10.1109/TGRS.2024.3397359.

Yangzhao Gong received the B.Sc. degree in surveying and mapping engineering from Xi'an University of Science and Technology, Xi'an, China, in 2015, the M.Sc. degree in surveying and mapping from Central South University, Hunan, China, in 2018, and the Ph.D. degree in land surveying and geo-informatics from The Hong Kong Polytechnic University, Hong Kong, China, in 2024.

His current research interests include atmospheric water vapor monitoring, numerical weather prediction, data assimilation, and Global Navigation Satellite System positioning.

Zhizhao Liu (Member, IEEE) received the B.Sc. degree in surveying engineering from the Jiangxi University of Science and Technology, Ganzhou, China, in 1994, the M.Sc. degree in geodesy from Wuhan University, Wuhan, China, in 1997, and the Ph.D. degree in geomatics engineering from the University of Calgary, Calgary, AB, Canada, in 2004.

He is currently a Professor with the Department of Land Surveying and Geo-Informatics, The Hong Kong Polytechnic University, Hong Kong. He has more than 30 years of experience in Global Positioning System (GPS)/Global Navigation Satellite System (GNSS) research. His group has developed a highly efficient and effective algorithm of cycle slip detection and repair for dual- and multifrequency GNSS carrier phase data. The algorithm his group developed can improve the accuracy of water vapor retrieval from remote sensing satellite data by up to 50%. His group developed China's first GPS precise point positioning (PPP)-based precipitable water vapor real-time monitoring system in the Pearl-River-Delta region in 2012. In 2012, his group established Hong Kong's first GPS/GNSS-based ionosphere scintillation monitoring system (two stations deployed in South and North Hong Kong) with his collaborators. His research group established Hong Kong's first GPS/GNSS-radiosonde water vapor sounding collocation system in 2013 in collaboration with Hong Kong Observatory. His research interests include new algorithm development for precise GPS, GNSS, GPS/GNSS PPP, ionosphere modeling and scintillation monitoring, tropospheric remote sensing and modeling, and GPS/GNSS meteorology.

Dr. Liu is the recipient of the inaugural Early Career Award of the Hong Kong Research Grants Council, Hong Kong, in 2012, and the inaugural Best Conference Paper of the China Satellite Navigation Conference, China, in 2013. In 2014, he was nominated by the Hong Kong Observatory for the World Meteorological Organization "Norbert Gerbier-MUMM International Award for 2015" for his article that has developed a method to evaluate the absolute accuracy of water vapor measurements.